

Quantum transport in the presence of a finite-range time-modulated potential

C. S. Tang¹ and C. S. Chu²

¹*Physics Division, National Center for Theoretical Sciences, P.O. Box 2-131, Hsinchu 30013, Taiwan*

²*Department of Electrophysics, National Chiao Tung University, Hsinchu 30010, Taiwan*

Quantum transport in a narrow constriction, and in the presence of a finite-range time-modulated potential, is studied. The potential is taken the form $V(x, t) = V_0 \theta(x)\theta(a - x) \cos(\omega t)$, with a the range of the potential and x the transmission direction. As the chemical potential μ is increasing, the dc conductance G is found to exhibit dip, or peak, structures when μ is at $n\hbar\omega$ above the threshold energy of a subband. These structures in G are found in both the small a ($a \ll \lambda_F$) and the large a ($a \gg \lambda_F$) regime. The dips, which are associated with the formation of quasi-bound states, are narrower for smaller a , and for smaller V_0 . The locations of these dips are essentially fixed, with small shifts only in the case of large V_0 . Our results can be reduced to the limiting case of a delta-profile oscillating potential when both a and V_0a are small. The assumed form of the time-modulated potential is expected to be realized in a gate-induced potential configuration.

PACS numbers: 72.10.-d, 72.40.+w

I. INTRODUCTION

Inelastic scattering processes in quantum transport have drawn continuous attentions in the recent past. One of the common model used is to invoke a time-modulated potential, with a certain spatial profile, to the system.^{1,2,3,4,5,6,7,8,9,10} This model was first utilized by Büttiker and Landauer¹ who, in considering a time-modulated barrier, attempted to extract a traversal time of a particle tunneling across the barrier. Later work from other groups have considered inelastic scatterings in different configurations such as the double oscillating barriers³, the time-modulated barrier with a delta profile^{4,5}, and the oscillating quantum well in between two static barriers^{7,8}. The model has also been extended to incorporate the inelastic effects due to phonons by introducing a time-modulated potential involving the phonon operators.^{11,12,13,14} In all these studies, the features arising from the inter-mixing between the elastic scattering, through a static potential, and the inelastic scattering, through a time-varying potential, is emphasised. In particular, these studies have demonstrated, among others, the interesting feedback effect of the inelastic scattering on the elastic channel. Even though the above model is appropriate only for inelastic processes that preserve the phase coherence of the transmitting particles, the model has practical importance because the coherent inelastic scattering (CIS) can be realized, at least, in the case when the time-modulated potential is well-specified.

A possible realization of CIS processes in nanostructures is expected to be found in gate-controlled quantum point contacts (QPC), as shown in Fig. 1. Similar gate-induced potential configuration has been suggested by Gorelik *et al.*,¹⁰ who considered microwave-induced effects on the Josephson current through a narrow constriction (NC). Their focus is on the resonance of the microwave frequency with the energy levels of the Andreev bound states formed in the NC, which has both ends connected to superconducting electrodes. For our

purposes here, a simple exhibition of the CIS is expected to be found readily in a normal state gate-controlled QPC. Recent development in the split-gate technology has made possible the fabrication of such gate-controlled QPC.^{15,16} The split-gates, when negative biased, define electrostatically a NC on a two-dimensional electron gas (2DEG). The dc quantum transport properties of these QPC systems has been studied intensively.^{17,18} More recently, there are growing interest in the time-dependent properties, such as the effects of photons, in these QPC systems.^{6,19,20,21,22,23} It is thus legitimate to consider the quantum transport in a NC which is acted upon by an additional, and ac biased, gate, as shown in Fig. 1. This ac biased gate, which is different from the split-gates that define the NC, induces on the NC a time-modulated potential. The scattering of the conduction electrons by this time-modulated potential is both coherent and inelastic.

There is another reason why quantum transport in a NC in the presence of a time-modulated, and gate-induced, potential is interesting. This is closely related to the density of states (DOS) structures in the NC. The energy levels in the NC are quantized into one-dimensional subbands so that the DOS is singular at the subband bottoms. In the presence of attractive impurities, such singularities in the DOS lead to dip structures in the dc conductance G , as the chem-

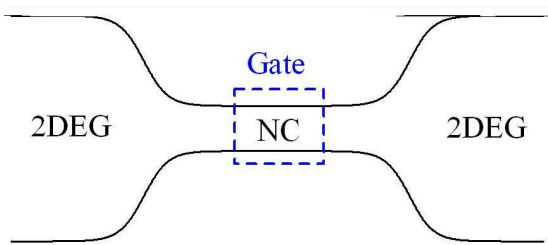


FIG. 1: Sketch of the gated QPC in which a NC is connected adiabatically at each end to a 2DEG electrode. The gate induced a finite-range time-modulated potential in the NC.

ical potential μ is increasing.^{24,25,26,27,28,29,30,31,32} The dip structures occur when μ is just below a subband edge. According to Bagwell,²⁵ these dip structures are associated with the formation of impurity-induced quasi-bound-states (QBS).²⁵ The wavefunction at this energy μ and in this subband is evanescent along the transmission direction. Hence for the case of an attractive impurity, a QBS splits off from each subband.²⁵ An electron originally in a propagating state in other subband can thus be scattered elastically into and be trapped by this QBS. This gives rise to dip structures in G .

The QBS features in G are found also when a point barrier oscillates in a NC.⁵ In this case, for a not-too-large oscillation amplitude, the dc conductance G exhibits dip, or peak structures when μ is at $n\hbar\omega$ above a subband edge. These structures correspond to the situation when the electrons can make transitions, via inelastic processes, to the QBS just below the subband edge. That there is QBS, induces by the point oscillating barrier, below each subband edge is demonstrated by Bagwell⁵ from the energy poles in the current transmission coefficients. The imaginary part of the energy poles are negative, which is consistent with the nature of the QBS. The existence of these QBS is again due to the singular DOS near a subband edge. It is important to ask whether such QBS features in G persist in the case of a finite-range time-modulated (FRTM) potential. This question has not been addressed before and, if the QBS features did persist in a FRTM potential, will have important implications to time-dependent properties of QPC systems. Furthermore, since the potential is expected to be gate-induced, the problem is within reach of the recent experimental capability.

In this paper, we simplify the problem by assuming the the gate-induced potential in the NC to be represented by the form $V_0\theta(x)\theta(a-x)\cos(\omega t)$, where a is the range of the potential and x is the transmission direction. Our simplification is in replacing the smooth longitudinal potential profile, of which the potential built up within a longitudinal distance of order λ_F , by an abrupt profile. The abruptness of the profile is expected to do nothing except introducing additional multiple scatterings between the two abrupt edges of the potential. This results in additional harmonics in G . Thus for the cases when the magnitude of these harmonics is small, our results are expected to resemble qualitatively the features in a smooth profile potential. An explicit smooth-profile consideration, however, is left to the further study.

Using this *small-harmonic-magnitude* criteria, we find the QBS features in G in both the small a ($a \ll \lambda_F$) and the large a ($a \gg \lambda_F$) regime. Our results can be reduced to the limiting case of a delta-profile oscillating

potential when both a and V_0a are small. In our calculation, the inelastic scattering is solved nonperturbatively. From our results, we note that even within the *small-harmonic-magnitude* criteria, the inelastic scattering has to be treated beyond one sideband approximation. The sideband index n labels those electrons which net energy change is $n\hbar\omega$.

In Sec. II we present the formulation for the inelastic scattering and the connection of the current transmission coefficients with the conductance G . In Sec. III we present numerical examples illustrating the QBS features in a FRTM potential. Finally, Sec. IV presents a conclusion.

II. THEORY

In this section, the inelastic scattering problem is formulated and the equations for the current transmission and reflection coefficients are obtained. The conductance G is then expressed in terms of these coefficients.

The QPC is modelled by a NC connecting adiabatically at each end to a 2DEG. Hence the transmission of the electrons into, or out of, the NC region is adiabatic.³³ The gate-induced potential is assumed to affect only the NC region of the QPC. Therefore we need only to formulate the inelastic scattering in the NC region. The NC is taken to have a quadratic transverse confinement potential $\omega_y^2 y^2$. The gate-induced potential is taken the FRTM form

$$V(x, t) = V_0 \theta(x) \theta(a - x) \cos(\omega t), \quad (1)$$

which connection with a smooth-profile potential has been discussed in the previous section.

Choosing the energy unit $E^* = \hbar^2 k_F^2 / 2m^*$, the length unit $a^* = 1/k_F$, the time unit $t^* = \hbar/E^*$, and V_0 in units of E^* , the dimensionless Schrödinger equation becomes

$$[-\nabla^2 + \omega_y^2 y^2 + V(x, t)] \Psi(\mathbf{x}, t) = i \frac{\partial}{\partial t} \Psi(\mathbf{x}, t). \quad (2)$$

Here k_F is a typical Fermi wavevector of the reservoir and m^* is the effective mass. The transverse energy levels are quantized, with $\varepsilon_n = (2n + 1)\omega_y$, and $\phi_n(y)$ the wavefunction. The FRTM potential is uniform in the transverse direction and does not induce inter-subband transitions, leaving the subband index n unchanged. Thus for a n th subband electron incident along \hat{x} , and with energy μ , the scattering wavefunction can be written in the form $\Psi_n^+(\mathbf{x}, t) = \phi_n(y) \psi(x, t)$, where³⁴

$$\psi(x, t) = \begin{cases} e^{ik_n(\mu)x} e^{-i\mu t} + \sum_m r_n(m) e^{-ik_n(\mu+m\omega)x} e^{-i(\mu+m\omega)t}, & \text{if } x < 0, \\ \sum_p [J_p(V_0/\omega) e^{-ip\omega t}] \int d\epsilon [\tilde{A}_n(\epsilon) e^{ik_n(\epsilon)x} + \tilde{B}_n(\epsilon) e^{-ik_n(\epsilon)x}] e^{-i\epsilon t}, & \text{if } 0 < x < a, \\ \sum_m t_n(m) e^{ik_n(\mu+m\omega)x} e^{-i(\mu+m\omega)t}, & \text{if } x > a, \end{cases} \quad (3)$$

and n, m are the final subband and sideband indices, respectively. The effective wavevector for an electron with energy ε and in the n th subband is given by $k_n(\varepsilon) = \sqrt{\varepsilon - (2n+1)\omega_y}$. The sideband index m corresponds to the net energy change of $m\hbar\omega$ for the outgoing electrons.

It is very important to note that had the length of the NC been infinite, and the range of the potential $V(x, t)$ were extended to cover the entire NC, the longitudinal wavevector k_n would be a good quantum number so that no *real* transition could have occurred. However, as long as $V(x, t)$ has a finite range, k_n is no longer conserved, and *real* transitions from $k_n(\varepsilon)$ to $k_n(\varepsilon \pm m\omega)$ are permitted for electrons traversing the potential. Thus the finiteness in the range of the time-modulated potential alone makes possible the absorption of energy by the electrons for arbitrary ω . This picture holds regardless of the range, long or short, and the profile, abrupt or smooth, of the potential. The mathematical statement of the above

physical picture turns out naturally, and given by Eq.(4), in the following.

The expressions for the reflection and the transmission coefficients can be obtained from matching the wavefunctions, and their derivatives, at the two ends of the FRTM potential. For the above matching to hold in all time, the integration variable ϵ in Eq.(3) has to take on discrete values $\mu \pm m\omega$. Hence we can write $\tilde{A}_n(\epsilon)$ and $\tilde{B}_n(\epsilon)$ in the form

$$\tilde{F}_n(\epsilon) = \sum_m F_n(m) \delta(\epsilon - \mu - m\omega), \quad (4)$$

of which $\tilde{F}_n(\epsilon)$ refers to either $\tilde{A}_n(\epsilon)$ or $\tilde{B}_n(\epsilon)$. After performing the matching, and the current reflection coefficients $r_n(m)$ eliminated, we obtain the equations relating $A_n(m)$, $B_n(m)$, and the current transmission coefficients $t_n(m)$,

$$t_n(m) = \sum_{m'} [A_n(m') e^{-iK_n^-(m, m')a} + B_n(m') e^{-iK_n^+(m, m')a}] J_{m-m'}(V_0/\omega), \quad (5)$$

$$k_n(\mu + m\omega) t_n(m) = \sum_{m'} k_n(\mu + m'\omega) [A_n(m') e^{-iK_n^-(m, m')a} - B_n(m') e^{-iK_n^+(m, m')a}] \times J_{m-m'}(V_0/\omega), \quad (6)$$

and

$$2k_n(\mu) \delta_{m0} = \sum_{m'} [A_n(m') K_n^+(m, m') + B_n(m') K_n^-(m, m')] J_{m-m'}(V_0/\omega), \quad (7)$$

where $K_n^\pm(m, m') = k_n(\mu + m\omega) \pm k_n(\mu + m'\omega)$. Equations (5)-(7) can be shown explicitly to reduce to the corresponding equations for the delta-profile time-modulated potential in the $a \rightarrow 0$ limit.³⁵

The zero temperature conductance is given by $G = (2e^2/h) \sum_{n=0}^N G_n$, where $G_n = \sum_m G_n^m$, and $N + 1$ is the number of propagating subbands in NC for the chemical potential μ . The contribution to G from electrons incident from subband n and transmit into sideband m is given by G_n^m , which is related to the transmission co-

efficients, given by

$$G_n^m = [k_n(\mu + m\omega)/k_n(\mu)] |t_n(m)|^2. \quad (8)$$

Solving Eqs.(5)-(7), we obtain $t_n(m)$, $A_n(m)$, and $B_n(m)$, using which the current reflection coefficient $r_n(m)$ can be calculated,

$$r_n(m) = \sum_{m'} [A_n(m') + B_n(m')] J_{m-m'}(V_0/\omega) - \delta_{m0}. \quad (9)$$

We solve the coefficients $r_n(m)$, and $t_n(m)$ exactly, in the numerical sense, by imposing a large enough cutoff to the sideband index. The correctness of our procedure is checked against the conservation of current condition, given by

$$\sum_m \frac{k_n(\mu + m\omega)}{k_n(\mu)} [|t_n(m)|^2 + |r_n(m)|^2] = 1. \quad (10)$$

III. NUMERICAL RESULTS

We calculate, in the following, the conductance G of a NC acted upon by a FRTM potential. The FRTM potential does not induce inter-subband transitions and so each occupied subband contributes independently to the total conductance. Thus it suffices for our purposes here to present the conductance of only one subband, which we take it to be the lowest one.

In this section, the behavior of G with respect to the chemical potential μ is studied. Since G depends also on the potential range a , and the oscillating amplitude V_0 , we present the behavior of G in four situations. Firstly, this G behavior is shown for a fixed while varying V_0 . Secondly, the G behavior is presented for a fixed $V_d = V_0 a$, while varying a . This is to make connection with the delta-profile results, in which the time-modulated potential is of the form $V_d \delta(x) \cos(\omega t)$. Thirdly, the G behavior for V_0 fixed, while a varying, is presented. The fourth situation is to compare the G behavior for different ω . In addition, we present the time averaged spatial distribution for the scattering state, of which the incident energy is very close to the QBS structure, and the QBS is about to occur. Finally, we compare the one-sideband approximation results with the nonperturbative results.

In our numerical examples, the NC is taken to be that in a high mobility $\text{GaAs-Al}_x\text{Ga}_{1-x}\text{As}$ with a typical electron density $n \sim 2.5 \times 10^{11} \text{ cm}^{-2}$, and $m^* = 0.067m_e$. Correspondingly, our choice of energy unit $E^* = \hbar^2 k_F^2 / (2m^*) = 9 \text{ meV}$, length unit $a^* = 1/k_F = 79.6 \text{ \AA}$, and frequency unit $\omega^* = E^*/\hbar = 13.6 \text{ THz}$. We also take $\omega_y = 0.035$, such that the effective NC width is of the order of 10^3 \AA . In the following, in presenting the dependence of G on μ , it is more convenient to plot G as a function of X instead, where $X = [(\mu/\omega_y) + 1]/2$. The integral value of X is the number of propagating channels.

In Figs. 2 and 3, G is plotted against X for a fixed, while V_0 is varying. The a is fixed at 150, 62, and 10 in Figs. 2, 3(a), and 3(b), respectively. The frequency ω is taken to be 0.014, which energy interval ω corresponds to an interval $\Delta X = \omega/(2\omega_y) = 0.2$ on the ordinate. The threshold, or the subband edge, is at $X = 1$. We note that in all the cases shown, a major dip structure occurs at $X = 1.2$, which corresponds to $X - \Delta X = 1$. This is the QBS features because the electron with energy at X can make transition to the subband edge by giving up an energy ω . We note also that, in general, for larger V_0 , the

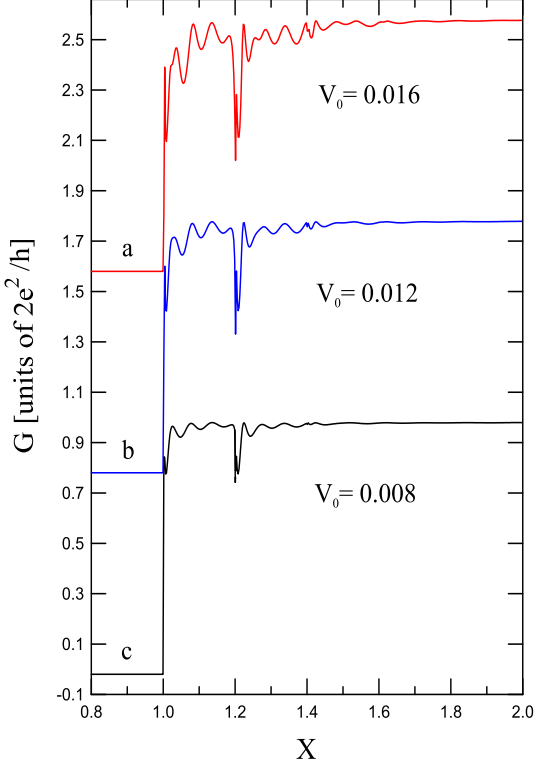


FIG. 2: Conductance G as a function of X for $a = 150$, and $\omega = 0.014$. The potential oscillating amplitudes are: “a” $V_0 = 0.016$, “b” $V_0 = 0.012$, “c” $V_0 = 0.008$. The curves are vertically offset for clarity.

structures at $X = 1 + N \Delta X$ are more evident. These are the situations when the electron can emit an energy of $N\omega$ and makes transition to the subband edge. The wavelength of the electron decreases as X is increasing. The relation is given by $\lambda = 2\pi/\sqrt{2\omega_y(X-1)}$. At the location of the first dip, when $X = 1.2$, we have $\lambda = 53$. Thus Fig. 2 corresponds to the case of a long potential range, with $a \simeq 2.8\lambda$, and Fig. 3(b) corresponds to the case of a short potential range, with $a \simeq 0.19\lambda$, near the occurrence of this first dip.

Besides the QBS features, there are harmonic structures in Fig. 2 and in Fig. 3(a). The structures are smaller for the lower V_0 . That these harmonics are associated with the multiple scattering between the abrupt edges of the potential can be identified from a resonance relation: $\lambda = 2a/n$, with n a positive integer. Correspondingly, the harmonic peaks are at $X_n = 1 + \Delta X_n$, with $\Delta X_n = (n\pi/a)^2/(2\omega_y)$. According to the above estimate, the first five harmonics are at $X_n \simeq 1.006, 1.025, 1.056, 1.1$, and 1.16 , which correspond quite reasonably to that in Fig. 2. However, for $X > 1.2$, the harmonic peaks correspond more closely to $X = 1.2 + \Delta X_n$. This can be explained as follows: the harmonics for $X > 1.2$ are contributed mostly from those electrons that give away an energy of ω so that the harmonics at X are very similar to that at $X - \omega$, or $X - 0.2$ for our

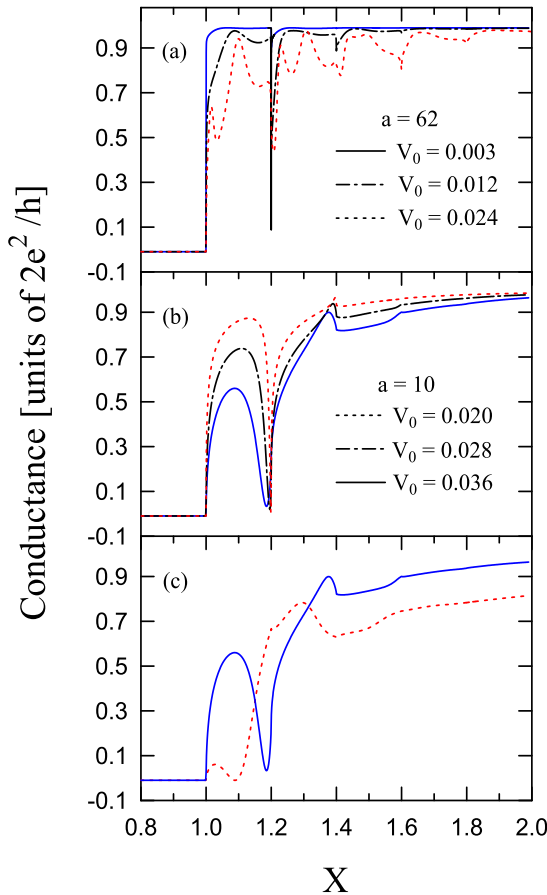


FIG. 3: G as a function of X , for $\omega = 0.014$. (a) $a = 62$, $V_0 = 0.003, 0.012, 0.024$; (b) $a = 10$, $V_0 = 0.020, 0.028, 0.036$; (c) FRTM potential result for $a = 10, V_0 = 0.036$ (solid curve). Delta-profile result for $V_d = 0.36$ (dashed curve).

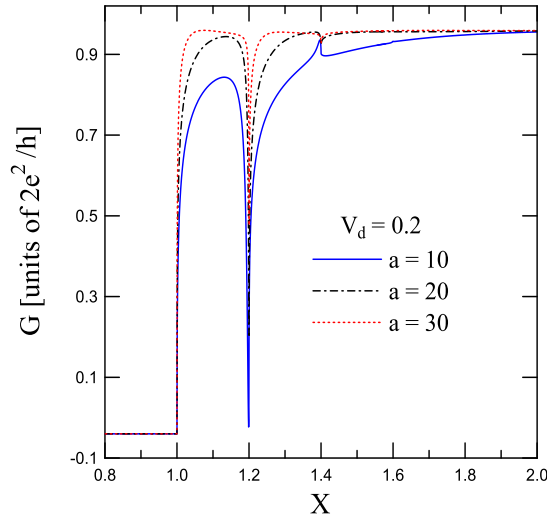


FIG. 4: G as a function of X for $V_d = 0.2$, and $\omega = 0.014$. The parameter $a = 10$ (solid curve); 20 (dash-dotted curve); 30 (dotted curve).

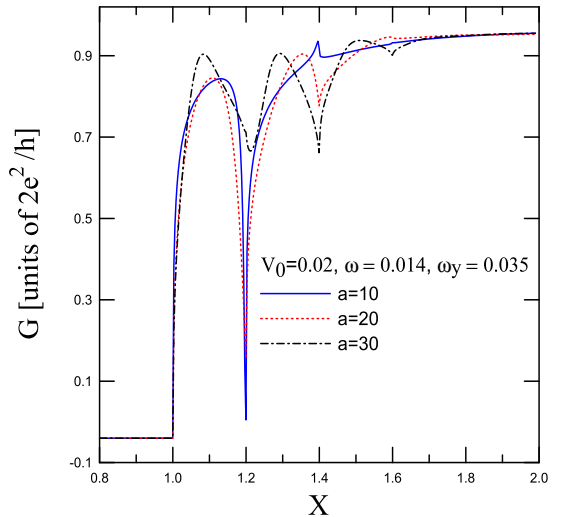


FIG. 5: G as a function of X for $V_0 = 0.02$, and $\omega = 0.014$. The parameter $a = 10$ (solid curve); 20 (dash-dotted curve); 30 (dotted curve).

cases. In Fig. 2, we see that the harmonic amplitudes are essentially smaller than the dip structure at $X = 1.2$. Using our *small-harmonic-amplitude* criteria, the QBS features are expected to be evident in a smooth-profile FRTM potential. Similar arguments can be applied to Fig. 3(a) to establish the harmonic peak locations, but we do not repeat the detail here. The harmonics are essentially suppressed for $V_0 = 0.003$, with a very narrow dip at $X = 1.2$. But at $V_0 = 0.012$, the harmonics are barely emerging, and there is a new dip structure developing at $X = 1.4$. At $V_0 = 0.024$, the harmonic amplitudes become very large. In the short potential range case, as shown in Fig. 3(b), the dip structure is narrower for the lower V_0 values. There is no harmonic structures and the dip location shift only slightly towards the lower X region in the larger V_0 case. Even though at $X = 1.2$, we have $a \simeq 0.19\lambda$, the result does not necessarily reduce to the delta-profile result. We point out that only the $V_0 = 0.02$ case in Fig. 3(b) corresponds to a delta-profile result for $V_d = V_0a = 0.2$. To demonstrate this, we show in Fig. 3(c) the $a = 10$, and $V_0 = 0.036$ result (solid curve), and compare with the delta-profile result for $V_d = 0.36$ (the dotted curve). The two curves are very different. The most important difference is that the dip location in the delta-profile case is shifted to $X \approx 1.1$ while the dip remains essentially unchanged for the FRTM potential.

To further establish the conditions when the FRTM potential result reduces to a delta-profile result, we show in Fig. 4 the FRTM potential result for a small $V_0a = 0.2$ value, while varying a . We recall that at $X = 1.2$, $\lambda \simeq 53$. The $a = 10$ result (solid curve) is identical with the delta-profile result. However, for $a = 20$, and 30 , the FRTM results are different from that of a delta-profile. As a is increasing, the dip at $X = 1.2$ becomes narrower and

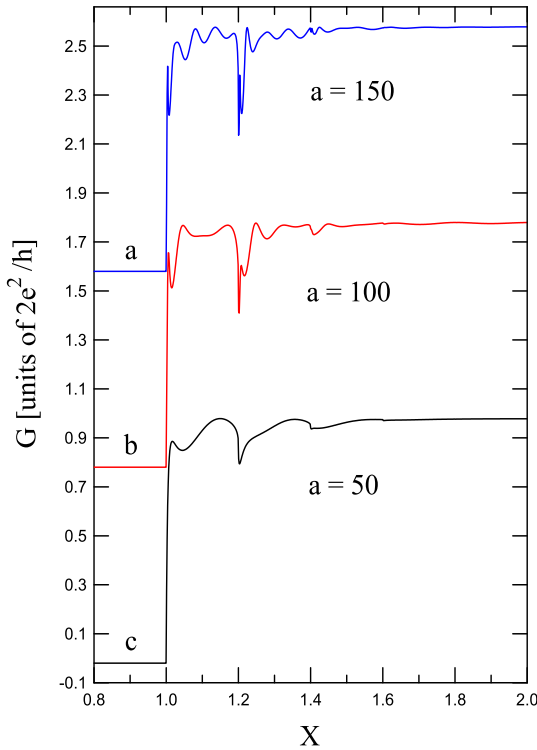


FIG. 6: G as a function of X for $V_0 = 0.012$, and $\omega = 0.014$. The interaction ranges are: “**a**” $a = 150$, “**b**” $a = 100$, “**c**” $a = 50$. The curves are vertically offset for clarity.

steeper, while the peak structure at $X = 1.4$ becomes a very shallow dip. This shows clearly that $a \ll \lambda$ must also be satisfied. Thus the correct conditions for a FRTM potential result to reduce to that of a delta-profile result are $a \ll \lambda$, and $V_0 a \ll 1$.

In Figs. 5 and 6, we fix V_0 at 0.02, and varying a . Fig. 5 is for the short potential range, with $a \leq \lambda$. Within this short a regime, the dip at $X = 1.2$ becomes wider and shallower, as a is increasing. The dip at $X = 1.4$, however, becomes more pronounced as a is increasing. These features indicate that high order processes such as the 2ω processes have become significant. An electron that is trapped can then be excited back out of the QBS. Thus we find the general trend that when the 2ω processes are significant, the first dip will become shallower. Fig. 6, on the other hand, is for the long potential range cases. Harmonics appear in the large a regime. We note that the $a = 50$ result, which corresponds to the case $a \simeq \lambda$, exhibits the emerging effects of the harmonics, and the dip structures become very shallow. For larger a , the dip structures become larger again.

In Fig. 7, we present the case for $a = 200$, $V_0 = 0.012$, and varying ω . In curve **a**, the dip structures are subjected to the effect of the harmonics, since at the dip location, the harmonic amplitude is not that small. However, for curves **b**, and **c**, the harmonic amplitudes are very small near the location of the dip. We point out also that the electron wavelengths λ near the dip structure

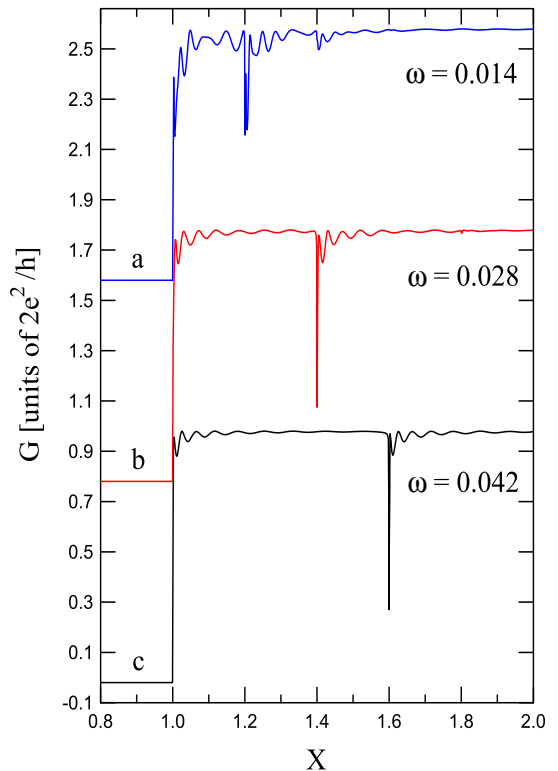


FIG. 7: G as a function of X for $a = 200$, and $V_0 = 0.012$. The frequencies are: “**a**” $\omega = 0.014$, “**b**” $\omega = 0.028$, “**c**” $\omega = 0.042$. The curves are vertically offset for clarity.

in the curves **b**, and **c**, are 37.6, and 30.7, respectively. Thus, for example, in curve **c**, $a \simeq 6.5\lambda$, and we are in the very long range regime. The QBS features are still very clear.

In Fig. 8, we plot the time-average of the spatial probability density for $a = 200$, $V_0 = 0.012$, $\omega = 0.028$, and $X = 1.399$. The dip location is at $X = 1.4$. Our choice of the parameters is near that for the occurrence of the QBS. The probability density shows the evanescent nature of the trapped electron. Furthermore, the higher probability density near the two edges of the FRTM potential shows that the QBS processes take place more frequently within a distance of order λ from the edges of the profile, at which spatial variation in the potential occurs.

Finally, in Fig. 9, we present the one sideband approximation results, together with our nonperturbative results. The deviation is large in the $X < 1.2$ region, which corresponds to the case when the evanescent modes play an important role. The deviation is larger for larger V_0 , as expected. This shows that the one sideband approximation is not appropriate and, in fact, the conservation of current condition is usually not satisfied.

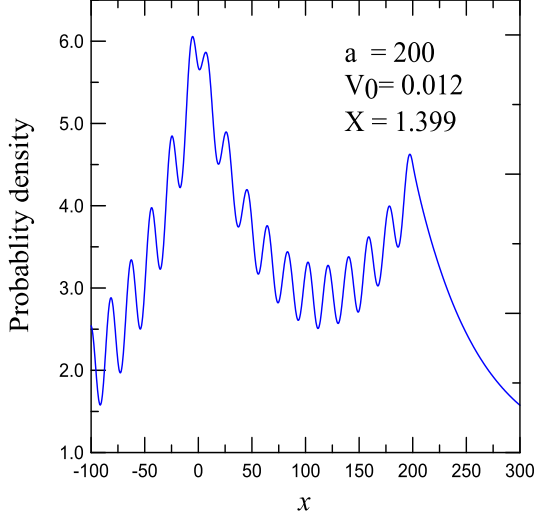


FIG. 8: Time-averaged probability density $\langle |\psi(x, t)|^2 \rangle$ as a function of longitudinal position x . The parameters are $a = 200$, $V_0 = 0.012$, and $X = 1.399$.

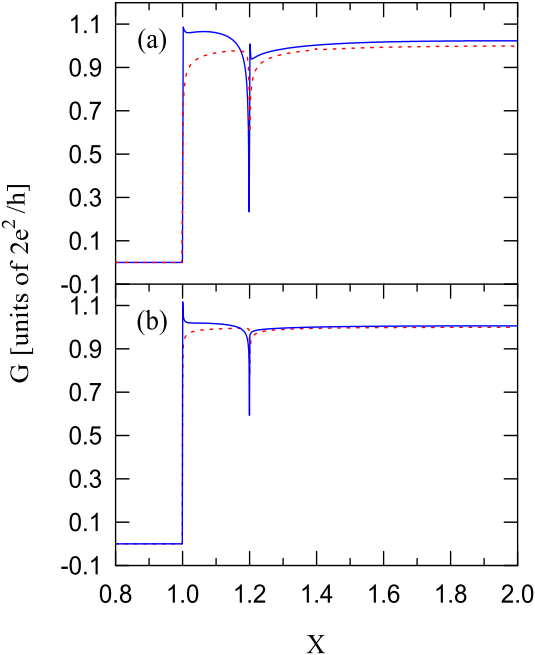


FIG. 9: G as a function of X for $a = 10$, and $\omega = 0.014$. Non-perturbative result (dashed curve) and one-sideband approximation result (solid curve). (a) $V_0 = 0.01$, (b) $V_0 = 0.005$.

IV. CONCLUSION

We have solved nonperturbatively the quantum transport in a NC, and in the presence of an abrupt-profile FRTM potential. The scattering process is both inelas-

tic and coherent. We find QBS features in all potential ranges, including the long as well as the short range regime. The dip structures associated with the QBS occur when μ is at $m\hbar\omega$ above the threshold of a subband edge. We find also that the inelastic processes occur more likely in the region when the potential profile varies spatially. In addition, from our results which we have not shown here, we find that a one-sideband approximation, in general, violates the conservation of current requirement.

We have presented arguments for the implications of our abrupt-profile FRTM potential results to that of a smooth-profile FRTM potential. We summarize and supplement our arguments, in the following, in light of the similarity and the difference between the two potential profiles. The abrupt-profile FRTM potential is similar to the smooth-profile FRTM potential in that they both break the longitudinal translational invariance. This allows the electrons to absorb or emit energy in units of $\hbar\omega$, for arbitrary ω . Consequently the electrons can make transitions, via inelastic processes, to the QBS just beneath a subband edge, giving rise in G to dip structures. A conclusion from this similarity between the profiles is that inelastic processes leading to QBS features are permitted in both of the profiles.

These two potential profiles are different, however, in that the abrupt-profile potential introduces additional multiple scatterings between the two abrupt edges of the potential, and gives rise to harmonics in G . Due to these additional multiple scatterings, the electrons effectively stay longer within the abrupt-profile FRTM potential region than within the smooth-profile FRTM potential region. As a result, the QBS features in the former potential profile might be perturbed, either being enhanced or suppressed. By proposing a *small-harmonic-magnitude* criteria, we attempt to look at cases where the perturbation from the harmonics to the QBS features is expected to be small. In these cases, the features of the two profiles are expected to be similar qualitatively.

In conclusion, the CIS and the QBS features are found in a NC, acted upon by an abrupt-profile FRTM potential. The features are argued to exhibit in the case of a smooth-profile FRTM potential, in particular, and is expected to affect the time-dependent properties of NC, in general. Further study, however, is needed to attain a better understanding.

Acknowledgments

This work was partially supported by the National Science Council of the Republic of China through Contract No. NSC85-2112-M-009-015.

¹ M. Büttiker, and R. Landauer, Phys. Rev. Lett. **49**, 1739 (1982).

² D. D. Coon, and H. C. Liu, J. Appl. Phys. **58**, 2230 (1985).

³ X. P. Jiang, J. Phys. Condens. Matter **2**, 6553 (1990).

⁴ M. Y. Azbel, Phys. Rev. B **43**, 6847 (1991).

⁵ P. F. Bagwell, and R. K. Lake, Phys. Rev. B **46**, 15329 (1992).

⁶ S. Feng, and Q. Hu, Phys. Rev. B **48**, 5354 (1993).

⁷ F. Rojas, and E. Cota, J. Phys. Condens. Matter **5**, 5159 (1993).

⁸ M. Wagner, Phys. Rev. B **49**, 16544 (1994).

⁹ V. A. Chitta, C. Kutter, R. E. M. de Bekker, J. C. Maan, S. J. Hawksworth, J. M. Chamberlain, M. Henin, and G. Hill, J. Phys. Condens. Matter **6**, 3945 (1994).

¹⁰ L. Y. Gorelik, V. S. Shumeiko, R. I. Shekhter, G. Wendum, and M. Jonson, Phys. Rev. Lett. **75**, 1162 (1995).

¹¹ B. Y. Gelfand, S. Schmitt-Rink, and A. F. J. Levi, Phys. Rev. Lett. **62**, 1683 (1989).

¹² W. Cai, T. F. Zheng, P. Hu, B. Yudanin, and M. Lax, Phys. Rev. Lett. **63**, 418 (1989).

¹³ W. Cai, P. Hu, T. F. Zheng, B. Yudanin, and M. Lax, Phys. Rev. B **41**, 3513 (1990).

¹⁴ J. M. Mohaidat, K. Shum, and R. R. Alfano, Phys. Rev. B **48**, 8809 (1993).

¹⁵ B. J. van Wees, H. van Houton, C. W. J. Beenakker, J. G. Williamson, L. P. Kouwenhoven, D. van der Marel, and C. T. Foxon, Phys. Rev. Lett. **60**, 848 (1988).

¹⁶ D. A. Wharam, T. J. Thornton, R. Newbury, M. Pepper, H. Ahmed, J. E. F. Frost, D. G. Hasko, D. C. Peacock, D. A. Ritchie, and G. A. C. Jones, J. Phys. C **21**, L209 (1988).

¹⁷ S. Washburn, and R. A. Webb, Rep. Prog. Phys. **55**, 1311 (1992).

¹⁸ F. A. Buot, Phys. Rep. **234**, 73 (1993).

¹⁹ A. Grincwajg, M. Jonson, and R. I. Shekhter, Phys. Rev. B **49**, 7557 (1994).

²⁰ Q. Hu, Appl. Phys. Lett. **62**, 837 (1993).

²¹ R. A. Wyss, C. C. Eugster, J. A. del Alamo, and Q. Hu, Appl. Phys. Lett. **63**, 1522 (1993).

²² L. Y. Gorelik, A. Grincwajg, V. Z. Kleiner, R. I. Shekhter, and M. Jonson, Phys. Rev. Lett. **73**, 2260 (1994).

²³ T. J. B. M. Janssen, J. C. Maan, J. Singleton, N. K. Patel, M. Pepper, J. E. F. Frost, D. A. Ritchie, and G. A. C. Jones, J. Phys. Condens. Matter **6**, L163 (1994).

²⁴ C. S. Chu and R. S. Sorbello, Phys. Rev. B **40**, 5941 (1989).

²⁵ P. Bagwell, Phys. Rev. B **41**, 10354 (1990).

²⁶ E. Tekman, and S. Ciraci, Phys. Rev. B **43**, 7145 (1991).

²⁷ J. A. Nixon, J. H. Davies, and H. U. Baranger, Phys. Rev. B **43**, 12638 (1991).

²⁸ Y. B. Levinson, M. I. Lubin, and E. V. Sukhorukov, Phys. Rev. B **45**, 11936 (1992).

²⁹ Y. Takagaki, and D. K. Ferry, Phys. Rev. B **46**, 15218 (1992).

³⁰ J. Faist, P. Guéret, and H. Rothuizen, Phys. Rev. B **42**, 3217 (1990).

³¹ C. C. Eugster, J. A. del Alamo, M. R. Melloch, and M. J. Rooks, Phys. Rev. B **46**, 10146 (1992).

³² C. S. Chu and M. H. Chou, Phys. Rev. B **50**, 14212 (1994).

³³ L. I. Glazman, G. B. Lesorik, D. E. Khmel'nitskii, and R. I. Shekhter, Pis'ma Zh. Eksp. Teor. Fiz. **48**, 218 (1988) [Sov. Phys. – JETP Lett. **48**, 238 (1988)]; A. Yacoby, and Y. Imry, Phys. Rev. B **41**, 5341 (1990).

³⁴ The wavefunction in the region $0 < x < a$ is, by construct, a solution of the time dependent Schrödinger equation, and has been proposed by Coon and Liu in Ref. 2, in their study of the time dependent quantum well tunneling.

³⁵ C. S. Chu and C. S. Tang (unpublished). The delta-profile time-modulated potential results, however, are given in Ref. 5.